Basic Principles and Clinical Applications of Magnetic Resonance Spectroscopy in Neuroradiology

Stephan Ulmer, MD,† Martin Backens, PhD,‡ and Frank J. Ahlhelm, MD‡*

Abstract: Magnetic resonance spectroscopy is a powerful tool to assist daily clinical diagnostics. This review is intended to give an overview on basic principles of the technology, discuss some of its technical aspects, and present typical applications in daily clinical routine in neuroradiology.

Key Words: magnetic resonance spectroscopy, basic principles, clinical indications, applications, neuroradiology

(*J Comput Assist Tomogr* 2015;00: 00–00)

Magnetic resonance imaging (MRI) has become the imaging modality of choice in neuroradiology because of its ability to provide high-resolution images of the gray and white matter and also visualize pathologic changes. MR spectroscopy (MRS)—as a noninvasive method—offers further information about metabolic processes such as energy metabolism, neuronal integrity, cell proliferation, and degradation as well as necrotic tissue changes. Without the need for a contrast agent, chemical structures and metabolites within the tissue can be measured and analyzed. In vitro MRS was performed many years before conventional MRI was implemented in daily clinical routine in the 1980s. This review gives a short technical overview of MRS, introduces typical clinical applications of the technique in daily routine in neuroradiology, and discusses some of its limitations and pitfalls.

On the basis of the physical principles of proton nuclear MRS (^{1}H-NMR), absorption of an electromagnetic impulse of an appropriate radiofrequency range generates different peak intensities, in contrast to absorption frequency, which is influenced by the molecular composition of the sample.[1–3] MR spectroscopy can detect metabolites at concentrations approximately 10,000 times lower than the abundant proton nuclei of fat and water molecules used in conventional MRI. In addition to hydrogen (^{1}H), MRS can generally be performed on many other nuclei or isotopes, too, for example, (^{15}N) nitrogen, (^{13}C) carbon, (^{19}F) fluorine, (^{23}Na) sodium, and (^{31}P) phosphorus; however, the technique might be hampered in some cases by its rather low sensitivity and low in vivo concentrations, thus leading to poor signal strength (Table 1).

Thus, as of now, phosphorus is the only other nucleus that is used for clinical applications. Phosphorus spectroscopy is technically challenging and generally used to investigate energy metabolism in muscle tissue but can also be performed to investigate the heart, liver, and brain.

For routine clinical applications, ^{1}H-NMR is best suited because of its concentration and resonance sensitivity. Furthermore, spatial resolution is better in a shorter acquisition time than for other nuclei. ^{1}H-MRS can be performed on a standard 1.5-T (or 3.0-T) scanner as a part of the routine protocol as no special hardware is required, such as additional coils or rearrangements.[5,6] The main compounds in the human brain (Table 2) are N-acetyl-aspartate (NAA), choline (Cho), and creatine (Cr).

The concentrations of these metabolites change depending on the underlying (pathologic) condition (see below). In daily routine, ratios of various metabolites are created as it is challenging to quantify metabolites accurately. Some metabolites can only be detected when their concentrations are significantly elevated, such as lactate in tumors or strokes, epilepsy, or mitochondrial pathologies; glycine in nonketotic hyperglycinemia; guanidinoacetate in guanidinoacetate methyltransferase deficiency; or elevated levels of phenylalanine in phenylketonuria.[7–11]

Basic Physical and Chemical Principles of MRS

Isotopes with an odd number of protons or neutrons have an intrinsic angular momentum, called spin, which is combined with a nuclear magnetic moment. The rate of the spin precesssion is characteristic when the probe is within a magnetic field, which is known as Larmor frequency. The Larmor frequency ω is linearly dependent on the field strength B:

$$\omega = \gamma \cdot B$$

The coefficient γ, called the gyromagnetic ratio, is a characteristic constant, which depends on the kind of nucleus. The Larmor frequencies of various nuclei in a magnetic field of 1.5 T can be found in Table 1. Hydrogen, as the most commonly used nucleus in clinical routine, has a Larmor frequency of 63.9 MHz at 1.5 T. After generating an electromagnetic impulse at their Larmor precession frequency (magnetic resonance condition), the nuclear spins induce an MR signal of the same resonant frequency that can be detected by the MR coil. Unlike MRI, a read-out gradient is not applied in MRS. The frequency information is used to identify the different chemical compounds, instead of spatial information as used in conventional MRI (Figs. 1 and 2).

The basic condition enabling MRS, in general, is the fact that an atomic nucleus placed in a magnetic field is partly shielded by the surrounding electron cloud. As a consequence, the local magnetic field at the site of the nucleus is slightly diminished depending on the exact composition of the electron cloud, which is formed mainly by adjacent atomic bonds. Because of their specific molecular bond, proton spins in different molecules will experience different shielding of the magnetic field. According to the relation $\omega = \gamma \cdot B$, changes in the magnetic field also alter the resonance frequency. This effect is called "chemical shift." The absolute frequency shift $\Delta\omega$ of the resonance frequency caused by a shielding σ (eg, a specific molecular bond) is directly proportional to the strength of the applied magnetic field B_0:

$$\Delta\omega = \sigma \cdot \omega_0 = \sigma \cdot \gamma \cdot B_0$$

The effective resonance frequency of a nuclear spin ω can be calculated as follows:

$$\omega = \omega_0 - \Delta\omega = (1 - \sigma) \cdot \gamma \cdot B_0$$

From the *Neuroradiology, Section of Medical Radiological Institute, Zurich, Switzerland; and †Department of Radiology and Neuroradiology, Institute of Neuroradiology, University Hospital Schleswig-Holstein, Kiel; and ‡Clinic of Diagnostic and Interventional Neuroradiology, Saarland University Hospital, Saarland, Germany.

Received for publication July 9, 2015; accepted July 21, 2015.

Correspondence to: Stephan Ulmer, MD, Department of Radiology and Neuroradiology, Institute of Neuroradiology, University Hospital Schleswig-Holstein, Schittenhelmstrasse 10, 24105 Kiel, Germany (e-mail: ulmer@email.com).

The authors declare no conflict of interest.

DOI: 10.1097/RCT.0000000000000322

TABLE 1. Important Nuclei for In Vivo MRS[4]

Nucleus	Larmor Frequency (1.5 T)	Relative Sensitivity (Nucleus)	Isotopic Abundance, %	Concentration In Vivo, mmol/L	Relative Signal In Vivo
^{1}H (water)	63.9	1	99.98	100 000	100
^{1}H (metabolites)	63.9	1	99.98	10	0.01
^{31}P	25.9	0.066	100	10	0.0007
^{23}Na	16.9	0.093	100	50	0.005
^{19}F	60.1	0.83	100	<1	<0.001
^{13}C	16.1	0.017	1.1	50	0.00001

Usually, chemical shifts are described as relative values (expressed in parts per million, ppm), which are independent of the field being applied:

$$\delta = \Delta\omega/\omega_0$$

For protons within a water molecule, the chemical shift is 4.7 ppm; for protons within fat tissue, the chemical shift is approximately 1.2 ppm, revealing a difference of 3.5 ppm. For a magnetic field strength of 1.5 T, this corresponds to 225 Hz.

Magnetic resonance signals are a function of time with exponentially decreasing high-frequency oscillation (ie, free induction decay [FID]; Fig. 1A). After Fourier transformation of the MR time signal, a specific frequency spectrum can be generated (Fig. 1B). The MR spectrum is a plot of the signal intensity of the previously defined voxel versus relative frequency shift δ. Chemicals or metabolites within the voxel are represented by different peaks at specific frequencies. For historical reasons, the direction of the frequency axis is chosen from right to left, that is, higher chemical shifts can be found on the left side on the MR spectrum.

Under ideal circumstances, each peak in an MR spectrum can be attributed to a specific metabolite. Relative quantities of these compounds can be calculated by determining the peak integral, that is, the area under the peak (Fig. 2).

There is no absolute value for these MR signals; thus, areas under individual peaks are not very accurate and may not be reproducible (see below). Therefore, relative quantification of metabolite concentrations can be achieved by calculating ratios of different peak integrals. It is quite difficult to determine absolute concentrations of the metabolites and would require additional measurements with phantom models as a reference. Although the area under the spectral peak is proportional to the metabolite concentration, the relationship is not immediate and depends on multiple biophysical parameters, including both pulse sequence parameters and metabolite relaxation times. Therefore, in clinical practice, relative concentrations and metabolite ratios are generally sufficient.

TABLE 2. Important Metabolites of the Central Nervous System

Metabolites	Chemical Shift, ppm	Interpretation/Marker/ Typically Found in
Water	4.70	
Inositol (Ins, mI)	3.54	Glial cells
Cho	3.22	Cell membrane, cell turnover
Cr	3.03 and 3.94	Energy metabolism
Glx	2.1-2.5 and 3.8	Neurotransmitter
NAA	2.02	Neuronal integrity
Alanine	1.5	Meningioma
Lactate	1.33	Anaerobic metabolism
Lipids	1.3-0.7	Necrosis; metastases

Field Strength Issues

As mentioned previously, plotting the signal intensity against the frequency of a chemical or metabolite within a given voxel at a certain magnetic field strength gives the MR spectrum. Higher

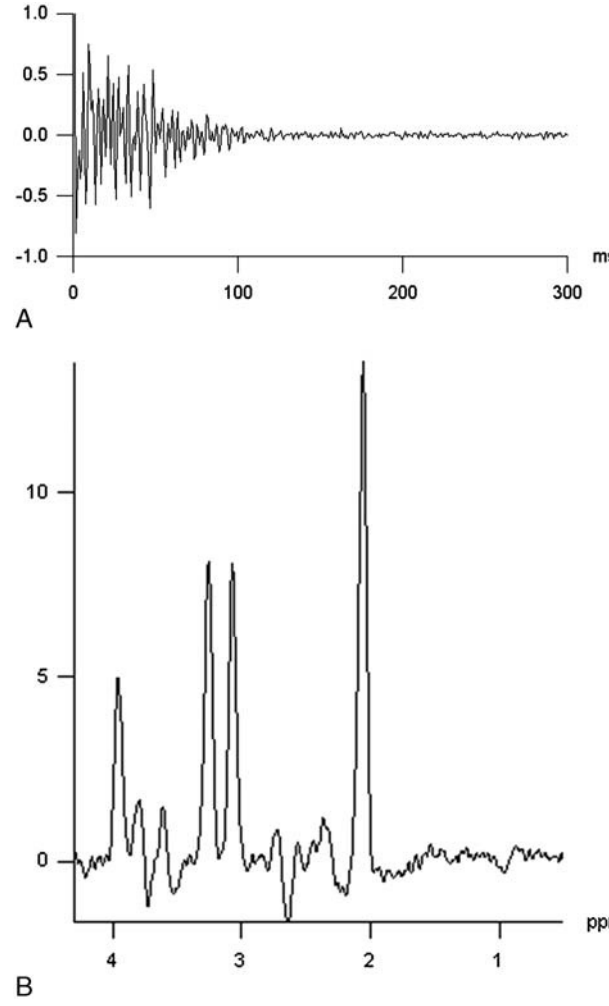

FIGURE 1. Magnetic resonance time signal. A, FID. B, Magnetic resonance spectrum after Fourier transformation.

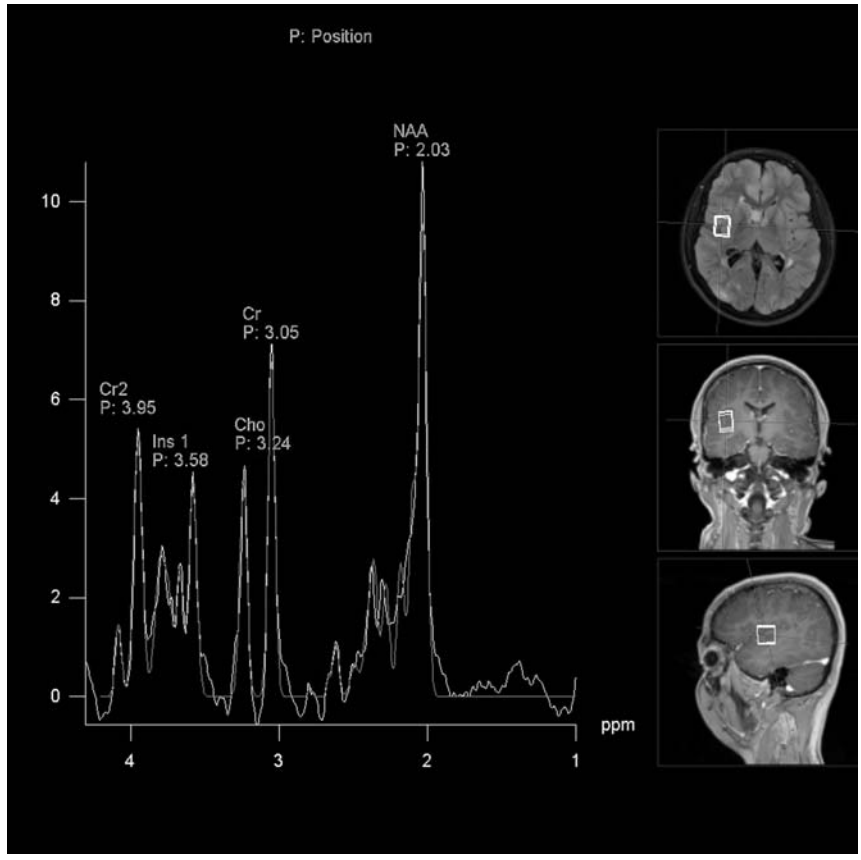

FIGURE 2. Magnetic resonance spectroscopy and MRI reference images (localization of the voxel) in a healthy volunteer. Cr2 indicates second peak of Cr.

magnetic field strengths increase the absolute chemical shifts, enabling a sharper delineation of the peaks within a spectrum. The signal-to-noise ratio (SNR) correlates (approximately) linearly to the magnetic field strength; thus, doubling the magnetic field strength from 1.5 to 3 T also increases the signal intensities of the peaks. Signal-to-noise ratio is often defined as the height of the largest metabolite peak divided by the root-mean-square amplitude of the noise in the spectrum. However, with higher field strengths, the susceptibility to field distortions caused by tissue inhomogeneity and magnetic impurities is also stronger, which impairs signal intensities. Thus, 3-T ^{1}H-MRS demonstrated an only 49% to 73% SNR increase in the cerebral metabolite signal and a slightly superior spectral resolution as compared with 1.5 T, but only at short echo time (TE) in brain tumors. Indeed, the signal and resolution were almost absent at intermediate TE. In their study, Kim et al[12] actually did not find any significant difference in the metabolite ratios between the 2 field strengths.

Sequence Protocols

For spectroscopic data acquisition, either single voxel (SVS) or multivoxel techniques (chemical shift imaging [CSI]) can be used. Multivoxel techniques cover a much larger area, which is helpful in visualizing lesions with various compounds or in metabolic disorders. Both 2- and 3-dimensional techniques are available. However, the disadvantage of CSI is that the SNR is significantly weaker than that of SVS, the signal being spread among adjacent voxels. In addition, more time is required for scanning. However, if a broader area needs to be covered, it is quicker to scan than to perform several SVS measurements. In SVS, usually cuboid voxels with a size of approximately 1.5 cm^3 are used to achieve a sufficient SNR. Here, 2 main techniques are used: stimulated echo acquisition mode (STEAM) and point-resolved spectroscopy (PRESS). Previously, STEAM was the only sequence that could be performed with short TE by which metabolites with short T2 relaxation times could be detected, such as inositol, glutamate, glutamine, and others. Today, short TEs can also be used in PRESS. In addition, the SNR for STEAM is only half that for PRESS, nor does STEAM show the useful lactate inversion for TE = 135 milliseconds (see below); thus, PRESS is now usually the preferred modality for spectroscopy.

Depending on the question being addressed, the TE is modified. Short-echo MRS with a TE of 20 to 35 milliseconds is better suited for detecting metabolites with short T2 relaxation times such as glutamine, glutamate, myoinositol (mI), and most amino acids, which are important for evaluating complex metabolic abnormalities. Long TE values are generally used for spectra to investigate NAA, Cr, and Cho concentrations.

Some metabolite peaks, for example, lactate, can change their shape and may be inverted depending on the technique or the TE value used at acquisition. At a low TE, the lactate double peak is positive using STEAM and PRESS technique. Using an intermediate TE of approximately 135 milliseconds, the lactate doublet peak is inverted using PRESS technique and virtually erased using STEAM technique. With a long TE (approximately 270 milliseconds), the lactate peak is again positive for both techniques. The reason for these confusing variations is that the lactate molecule has 2 different resonances, one at 1.3 ppm and another at

4.1 ppm, arising from the protons in the methyl group (CH_3) and in the methine group (CH). The peak at 4.1 ppm is usually not visible in vivo because it is too close to the water peak. Because of interactions between the 2 groups—called J-coupling—the methyl resonance at 1.3 ppm is split into a doublet with a coupling constant of $J = 7.4$ Hz. The corresponding difference in Larmor precessional frequencies between the doublet components causes a periodical change of inphase and antiphase conditions depending on the TE. Using PRESS, the doublet is inphase at TE = $1/J = 135$ milliseconds but inverted relative to the other (uncoupled) resonances. At TE = $2/J = 270$ milliseconds, the doublet is also inphase but positive (not inverted). Signal variation in STEAM techniques depending on the TE is substantially more difficult because multiple quantum effects need to be considered.

The concentration of water is 10^4 to 10^5 times higher than any of the metabolites of interest. Thus, the water signal must be adequately suppressed, which can be achieved using a chemically selective saturation radiofrequency pulse applied at the water resonance before implementing the selected localization technique.[13] Furthermore, shimming before the measurement gives a more homogeneous magnetic field within the voxels, reducing spectral peak broadening and improving the SNR.

Because of the low sensitivity of NMR and the low concentration of metabolites (approximately 1-10 mmol/L), multiple signal acquisitions generally need to be averaged to obtain sufficient spectral quality.

If the 4 main peaks of a spectrum (Ins, Cho, Cr, and NAA) are connected by a manually drawn line, the angle with respect to the x-axis is 45° in healthy subjects, an angle referred to as Hunter angle (Fig. 3). As a rule of thumb, that roughly applies for spectra of the brain using STEAM and short TEs. However, as the appearance of spectra is influenced by various factors, including sequence parameters and localization, Hunter angle should only be used with great caution.

Postprocessing

After acquiring an MR signal, several postprocessing procedures are needed to qualitatively interpret and quantitatively analyze the MR spectra (FID; Fig. 1A). Nowadays, these steps are fully or partially automated by the scanner evaluation software.

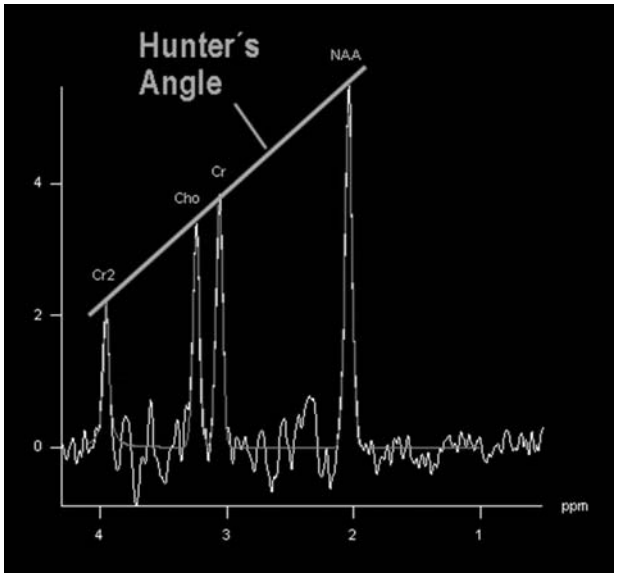

FIGURE 3. Hunter angle.

Pathological conditions change spectra; thus, "normal" peaks may be absent, or additional peaks can be depicted, which may require additional manual optimization in postprocessing. Particularly, when large amounts of different spectra are acquired using CSI, manual postprocessing can be rather demanding. In the first step, the MRS signal intensity is multiplied by a Gaussian or exponential function to decrease noise. A minor disadvantage of this filter process ("apodization") is that the lines are slightly broadened. This is followed by what is known as "zero filling," that is, the MRS signal is prolonged, resulting in a "smoother" appearance of the MR spectrum.

The most important step in postprocessing, however, is "Fourier transformation," which transforms the MR time signal into a frequency spectrum. After correcting baseline distortions, phase shifting is performed as a final step to achieve a pure absorption spectrum.

Characteristics Influencing Spectra

In addition to age (see below), other characteristics may also influence the spectra, including topography or sex, although the literature is somewhat incongruous in this regard. Neither Komoroski and coworkers[14] nor Raininko and Mattsson[15] found any differences between women and men, whereas Wilkinson and coworkers[16] found NAA and Cr to be higher in women than in men compared with Cho being higher in men than in women. Using a phantom, left-right asymmetries of up to 6.5% were observed, which was even more pronounced in healthy volunteers depending on the region of interest.[17] Variations between the left and right hemisphere were between 11% in the parietal lobe to 42% in the cerebellum for NAA-Cr. Maximum variations were found in Cho-Cr ratios of up to 72% in the parietal lobe. Only in the thalamus and cerebellum were no statistically significant left-right asymmetries observed, whereas there was a significant asymmetry for NAA-Cr in the parietal lobe, for Cho-Cr in the occipital lobe, for Cho-Cr and NAA-Cr in the temporal lobe, and for NAA-Cr in the frontal lobe.[17] These regional variations were also found by Komoroski and coworkers,[14] with lower values of Cho-Cr in the basal ganglia. Reproducibility represents another major issue. According to both phantom studies and examinations in healthy subjects, there was significant variation within runs and even more so in studies performed on separate days, which ranged from 9% to 18% for individual metabolites and from 10% to 26% for metabolite ratios in the parietal lobe. Even in sequentially performed examinations in the same location in 1 session, variations of up to 17% were observed for both metabolites and ratios.[18] All these sources of systemic error need to be borne in mind when interpreting results. Motion of the head or subject during the scan can further hamper the results. Physiological brain motion is unlikely to significantly influence the findings.[19] However, further motion leads to voxel misregistration, phase or frequency variations, phase dispersion, amplitude variation, and out-of-voxel contamination, all leading to line-shape deterioration and reduced SNR.[19–21]

Clinical Applications for MRS

Brain Development and Maturation

A variety of metabolites can be measured using MRS in vivo; however, as voxels contain heterogeneous cell populations, these metabolites may vary according to the chosen location and, thus, combination of cell types. In the healthy adult brain at 1.5 T, NAA (synthesized in brain mitochondria) shows the most prominent peak at 2.02 ppm, followed by Cr at 3.03 (and 3.94) ppm and Cho at 3.22 ppm.[22,23] N-acetyl-aspartate is a marker for intact

neurons (also thought to be involved in myelinization) that is not found in astrocytes or oligodendrocytes. Choline is found in astrocytes and even more so in oligodendrocytes, as are both Cr and NAA.[24]

Creatine (thought to represent energy metabolism) increases rapidly before and around birth (at term[24]). During further brain maturation, levels of NAA and Cr rise within the first 3 months of life, and mI declines, whereas Cho (thought to represent membrane, phospholipid, and myelin metabolism) shows a peak at 3 months with a decline thereafter toward early childhood.[25] At 6 months old, NAA is the most prominent detectable marker.[26–28] Choline decreases until the age of 3 years.[26]

In the healthy brain, lactate concentrations are below the detectability of MRS. It is a terminal metabolite of glycolysis. Whenever mitochondrial respiration is insufficient and energy is dependent on glycolysis, lactate rises as a result of less efficient energy production. It can be detected in the preterm (weeks 26-32) brain,[29] concentrations increasing with decreasing gestational age and degree of growth restriction.[30] The occipitoparietal regions seem to be more vulnerable than the basal ganglia.[31] In preterm infants, NAA was significantly lower if white matter abnormalities were present and lactate also correlated with the Apgar score.[32]

During further maturation, only moderate changes are observed in metabolites, including NAA (by approximately 50% from infancy to adulthood) and Tau in gray matter. In white matter, the total NAA concentration gradually increases during childhood and adolescence by approximately 30%. In the cerebellum, there is a developmental increase in NAA, whereas Tau, for which overall concentrations are highest in the cerebellum, decreases. In the thalamus, the concentrations of tCr and Tau are elevated in early infancy in comparison with constant levels in children and adults, accompanied by a developmental increase in tNAA.[33] From adolescence to old age, NAA, mI, and glutamine/glutamate (Glx) decrease.[15]

Noxa During Pregnancy

In children with fetal alcohol spectrum disorder, Cho (as a marker of phospholipids and myelin metabolism) was reduced as compared with controls. There was also a correlation between reduced Cho and reduced brain volume, suggesting white matter damage.[34] Another study found elevated NAA concentrations, probably as compensation in myelinization.[35]

In the children of mothers who smoked during pregnancy, significantly lower concentrations of mI (as a marker for glial cells) and Cr (a marker for energy metabolism, which is usually a very stable metabolite in MRS) were found.[36]

Asphyxia

Lactate and reduced NAA were found in children with asphyxia, which correlated with a poor neurological outcome.[37–41] As NAA is low at birth (see above), lactate seems to be more relevant.[42] As the end product of anaerobic metabolism, lactate can persist in the brain. In children with neurodevelopmental impairment, lactate was still found 1 year after perinatal asphyxia.[43,44]

Developmental Delay

Findings in children with developmental delay are not congruent throughout the literature. Normal finding compared with age-matched controls was reported.[45,46] Other studies found decreases in the NAA-Cr ratio, a marker for immature or ceasing neurons, and increased Cho-Cr as a marker for increased cell turnover.[47] A reduction in NAA was also found in another study.[48] Following up on children with idiopathic developmental delay, NAA remained reduced at the age of 9 to 10 years.[49] In children with congenital heart disease, NAA increased significantly slower during further development within the third trimester compared with controls.[50] There is further discordance in the literature with regard to autism. Compared with controls, lower levels of NAA, Cr, and Cho were found.[51,52] In later childhood (at 9-10 years old[49]) and in adulthood,[53] this was no longer apparent. Other studies found increased values of mI and Cho but no significant differences in NAA compared with controls[54] or even no evidence for brain mitochondrial dysfunction in children with autism[55]; thus, caution should be exercised in interpreting data concerning age-dependent fluctuations in metabolite levels.[56]

Mitochondrial Disorders

In patients with mitochondrial myopathy, encephalopathy, liver acidosis, and strokelike lesions, a significant Cho and NAA reduction was found. Lactate was not present in normal-appearing white matter.[57] The authors discussed whether Cho might represent a metabolic correlate for impairment or maintenance of membrane metabolism due to reduced energy production. Choline reduction could be reversed after short-term treatment with dichloroacetate.[58] Reduction in NAA represents neuronal loss. In patients with Leigh syndrome, reduced levels of NAA and Cr were noted, and lactate was observed in affected areas.[57,59,60]

Leukodystrophies

In the differential diagnosis of leukodystrophies, MRS might be helpful; however, changes in the metabolite ratios or levels are not specific for a certain disorder. Increased levels of mI and lactate and reduced NAA levels have been reported in Alexander disease.[61,62] Increased levels of NAA have been found in Canavan disease,[63] but other studies did not find any significant changes.[64] However, increased NAA is thought to be a biomarker for white matter diseases such as Pelizaeus-Merzbacher disease and Canavan disease.[65] Increased levels of NAA and increased mI and Cr, together with a reduction in Cho, were found in Pelizaeus-Merzbacher disease.[66] Both NAA and lactate levels were reduced in Krabbe disease. Increased ratios of Cho-Cr were found in Gaucher disease that correlated negatively with the impairment.[67]

Posttraumatic Changes

Posttraumatically, MRS may depict neuronal damage when NAA levels are decreased.[68,69] Furthermore, Cho was found to be increased initially. Then, NAA increased, whereas Cho decreased over time.[70] This opens new options in monitoring child abuse (nonaccidental trauma), as NAA was significantly decreased in these children.[71]

Brain Tumors

One of the main applications of MRS in adults is still brain tumor imaging. Initial experiments were performed in an animal model in the late 1990s, later applying MRS in brain tumors in humans in vivo. The animal model (C6 glioma) revealed an NAA decrease, a Cho increase, and a peak in lactate and lipids.[72] A variety of groups then used MRS to further characterize human brain tumors.[73–78]

In addition to detecting differences in the spectra of tumors and normal brain parenchyma, MRS was increasingly used for differential diagnosis of tumors. In general, tumors of glial origin show increased Cho (increased turnover) compared with Cr and a decrease in NAA due to neuronal loss. A ratio of 2:1 Cho-Cr is taken for diagnosing high-grade gliomas, being a cutoff to

distinguish them from low-grade lesions. Lactate and lipids are only found in higher grade lesion due to necrosis and anaerobic metabolism (Fig. 4). In metastasis (Fig. 5) and also in meningiomas (Fig. 6), NAA is usually only present if normal brain tissue is incorporated within the voxel of interest.[73,77,79–88]

Distinguishing low-grade lesions can be difficult. However, increased Cho was more likely to be found in WHO II lesions.[89]

Nonenhancing lesions in conventional MRI represent another challenge. Nonenhancing high-grade lesions could be distinguished from low-grade lesions by increased Cho and Cho-Cr ratios in several studies.[90–93]

Contrast-enhancing lesions, on the other hand, can also be a challenge as they could be lymphoma, glioblastoma, or metastasis. Ratios of lactate-lipids–Cr may help to differentiate these tumor types, with lymphoma having the highest values followed by glioblastomas and then metastasis.[94]

Magnetic resonance spectroscopy has also been used for predicting outcome in brain tumors. Lactate was found, for

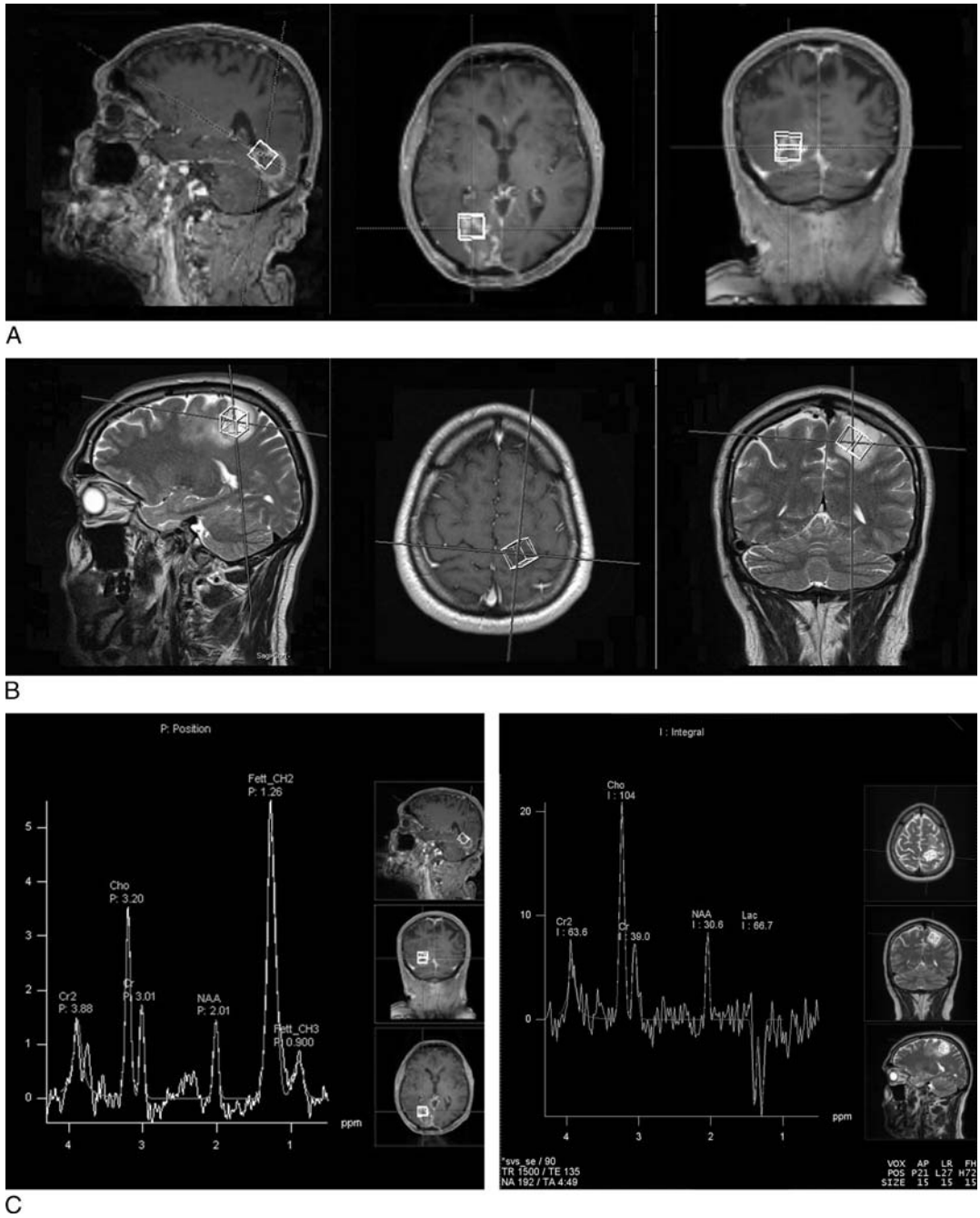

FIGURE 4. Magnetic resonance images (A) and MRS (C, left) of a glioblastoma. Reduced NAA is found due to neuronal degradation; increased Cho indicates cell proliferation. There are strong lipid peaks, which are typical in high-grade tumors. Magnetic resonance images (B) and MRS (C, right) of a nonenhancing WHO grade III astrocytoma. Choline is increased because of high cell turnover with anaerobic metabolism (lac peak). N-acetyl-aspartate is reduced because of destruction of normal brain tissue.

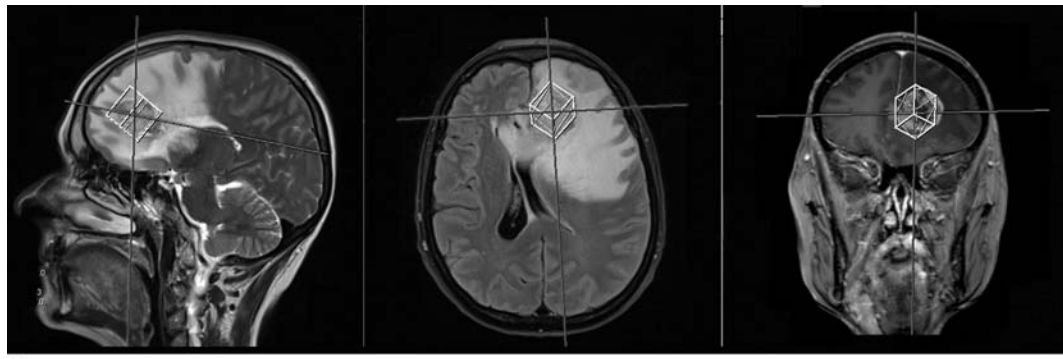

A

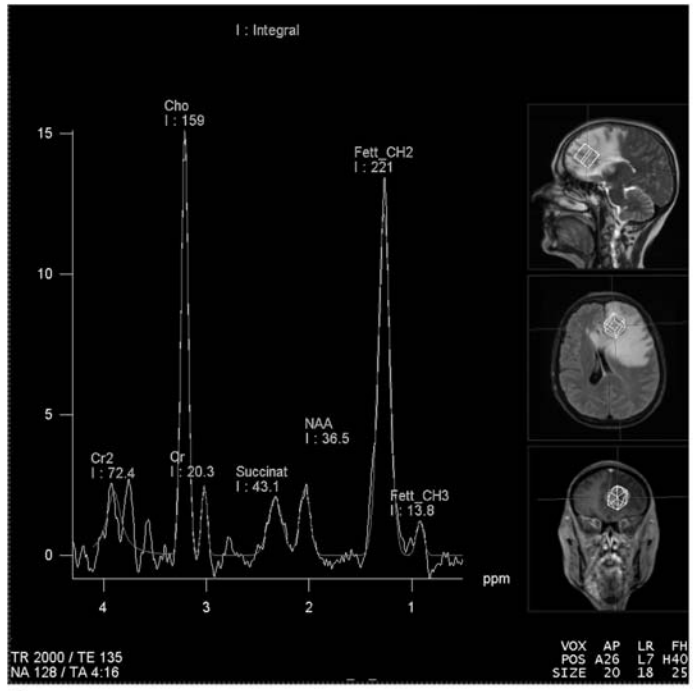

B

FIGURE 5. Magnetic resonance images (top row) and spectrum (bottom row) of metastasis from bronchial carcinoma. N-acetyl-aspartate as a neural marker is reduced; Cho is highly increased. Succinate and lipid peaks (CH_3 and CH_2) can be depicted because of necrosis.

example, in pontine gliomas with significantly worse outcome or if Cho-NAA changed.[83,95,96] In general, presence of lactate seems to be a predictor for worse outcome.[83,88,95,96]

As we know from biopsy-proven studies in which samples are taken from the rim of the resection cavity during tumor removal, tumor borders as defined by conventional MRI do not reflect the real extent of a lesion—neither by an area of signal intensity increase in T2-weighted images in low-grade lesions nor by the contrast-enhancing part of high-grade tumors. Magnetic resonance spectroscopy was also able to define these areas of tumor infiltration beyond the conventional imaging findings.[97]

In addition to initial diagnostic imaging, MRS is also used for follow-up examinations. Response to treatment could be predicted by a decrease in Cho-Cr at 14-month follow-up.[98] Before MRI or clinical deterioration, these changes can be depicted by MRS[99] and might be used to estimate response to therapy, overall survival, or time to progression.[100] Patients under antiangiogenic drugs have also been monitored using MRS. In patients in whom the decline in Cho was stronger, NAA increased, and lactate/lipids decreased, overall survival was higher.[101]

Magnetic resonance spectroscopy can also help with another common diagnostic problem during follow-up monitoring of patients with brain tumor: distinguishing recurrent disease from contrast-enhancing postradiation necrosis after radiation therapy. Compared with radiation necrosis, Cho-Cr was significantly increased in recurrent tumors,[102,103] with a cutoff of 1.8.[104]

The implementation of intraoperative MRI has opened new fields of research and clinical applications. At any time during the resection of a brain lesion, an early resection control can be performed. Such imaging is, however, hampered by the fact that surgical manipulation temporarily disrupts the blood-brain barrier, causing contrast enhancement of the rim of the resection cavity. Intraoperative dynamic susceptibility contrast-enhanced MRI[105,106] could reliably depict residual tumor. Magnetic resonance spectroscopy can also identify residual tumor intraoperatively with a sensitivity of 85.7% and a specificity of 100%.[107]

Parkinson Disease

In Parkinson disease (PD), any additional imaging modality is highly appreciated to facilitate diagnosis as there are no definite

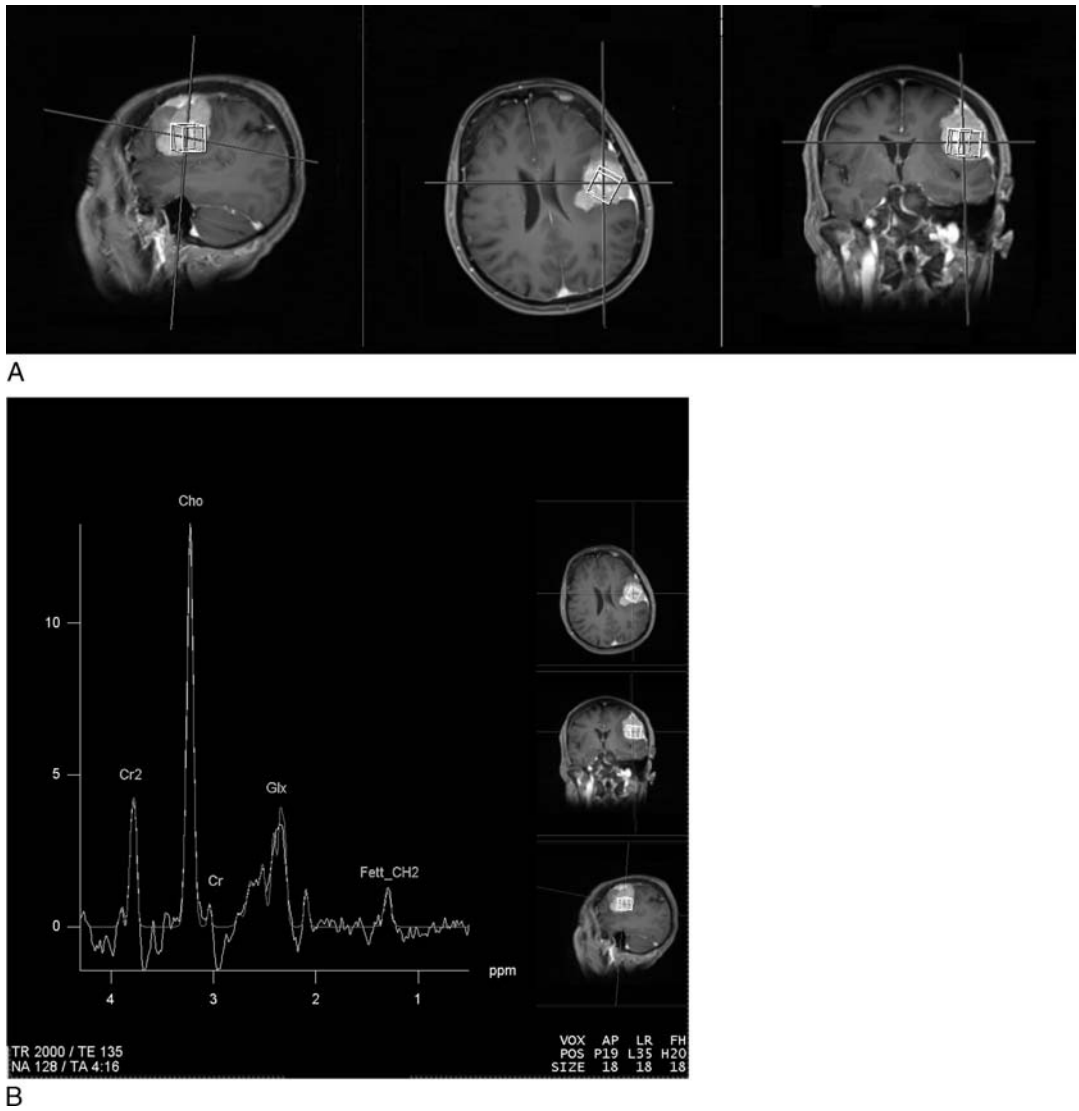

FIGURE 6. Magnetic resonance images (top row) and MRS (bottom row) of a meningioma. As this is an extra-axial lesion, the neuronal marker NAA is missing. There is almost no Cr and a small lipid peak (CH_2) but elevated Glx components (B).

signs in conventional MRI. Compared with controls, Cr was significantly lower in the substantia nigra in PD.[108] Other studies found NAA-Cr to be significantly reduced in the substantia nigra,[109,110] most likely as a sign of neuronal loss.

This is also true for other neurodegenerative disorders, such as multisystem atrophy and progressive nuclear palsy,[111] where NAA was found to be significantly decreased in the pallidum, putamen, and lentiform nucleus of these patients. Mapping glutamate and glutamine in the lentiform nuclei demonstrated reduced levels, suggesting that more than half of the dopaminergic neurons in the nigrostriatal projection must be lost before the onset of PD.[112] Mitochondrial dysfunction in mesostriatal neurons is thought to represent an early change in the pathogenic cascade in PD. Reduction of adenosine triphophosphate and phosphocreatine as final acceptors of energy from mitochondrial oxidative phosphorylation was found in the putamen and midbrain.[113] Reduced NAA-Cr and increased Cho-Cr and mI were found in the posterior cingulated gyrus in patients with PD compared with controls[114,115] as was a lower Glu-Cr ratio than in controls.[116] The NAA-Cr ratio was significantly lower in the pre-supplementary motor area in PD than in controls, too.[117]

Parkinson disease may show different clinical manifestations. Some are associated with cognitive decline. NAA-Cr was reduced in the occipital lobe of PD with mild cognitive impairment (MCI) compared with healthy controls. The Cho-Cr ratio was higher in the posterior cingulated gyrus in PD with MCI than in PD without MCI.[118] Magnetic resonance spectroscopy in the right dosolateral prefrontal cortex yielded reduced NAA ratios in patients with MCI; NAA in the left hippocampus was significantly reduced if they experience dementia.[119] Lower NAA-Cr and Glu-Cr ratios were found in PD with dementia than in controls in the posterior cingulated gyrus, and lower Glu-Cr ratios were found in PD with dementia than in PD without dementia.[114] Furthermore, the ratio of NAA-Cr correlated with the mental status in PD with dementia.[115] In the occipital region, NAA levels were significantly reduced in PD with dementia compared with PD without dementia and controls, which again correlated with neuropsychological status.[120]

Stroke

Although MRS does not play any role in decision making for further patient management in an acute stroke setting,[121] it may help to further understand underlying changes in the course of the disease. As knowledge of early changes after stroke onset is based on animal models for the most part, data for humans are limited. N-acetyl-aspartate is a key player in both the infarcted and noninfarcted areas. Indeed, as a marker of neuronal integrity, NAA decreased rapidly within the first 6 hours after the insult in an animal model followed by a slower decay thereafter.[122,123] On the other hand, however, recovery of NAA has been reported in an animal model with transient MCA occlusion despite histologically proven, persistent neuronal loss of up to 90% in the ischemic core.[124] As a marker, lactate is usually not present in healthy controls and increases as an end product of anaerobic glycolysis (Fig. 7).[121] However, in transient ischemia, additional metabolites such as glutamine and glutamate may predict irreversible lesions already 3 hours after ischemia.[125] In patients with motor impairment due to subcortical stroke in a chronic state, NAA was significantly reduced in the corresponding M1 compared with controls. Furthermore, the unaffected contralateral side also demonstrated lower NAA values than in controls. Myoinositol as a marker of glial involvement was increased.[126] N-acetylaspartate was also found to be lower in ipsilateral premotor areas.[127] Reduced blood supply caused by stenosis or occlusion of supplying vessels resulting in transient neurological deficits already leads to a reduction of NAA in the noninfarcted centrum semiovale.[128] Altered NAA was furthermore found to be more likely in patients with poorer recovery after stroke.[127]

Infections

Human Immunodeficiency Virus

Some human immunodeficiency virus research has included MRS. As early as 8 days after infection, MRS was performed and demonstrated increased Cho-Cr levels as signs of acute infection, frequently accompanied by headache during the acute retroviral syndrome.[129] Furthermore, Cho-Cr was increased in untreated

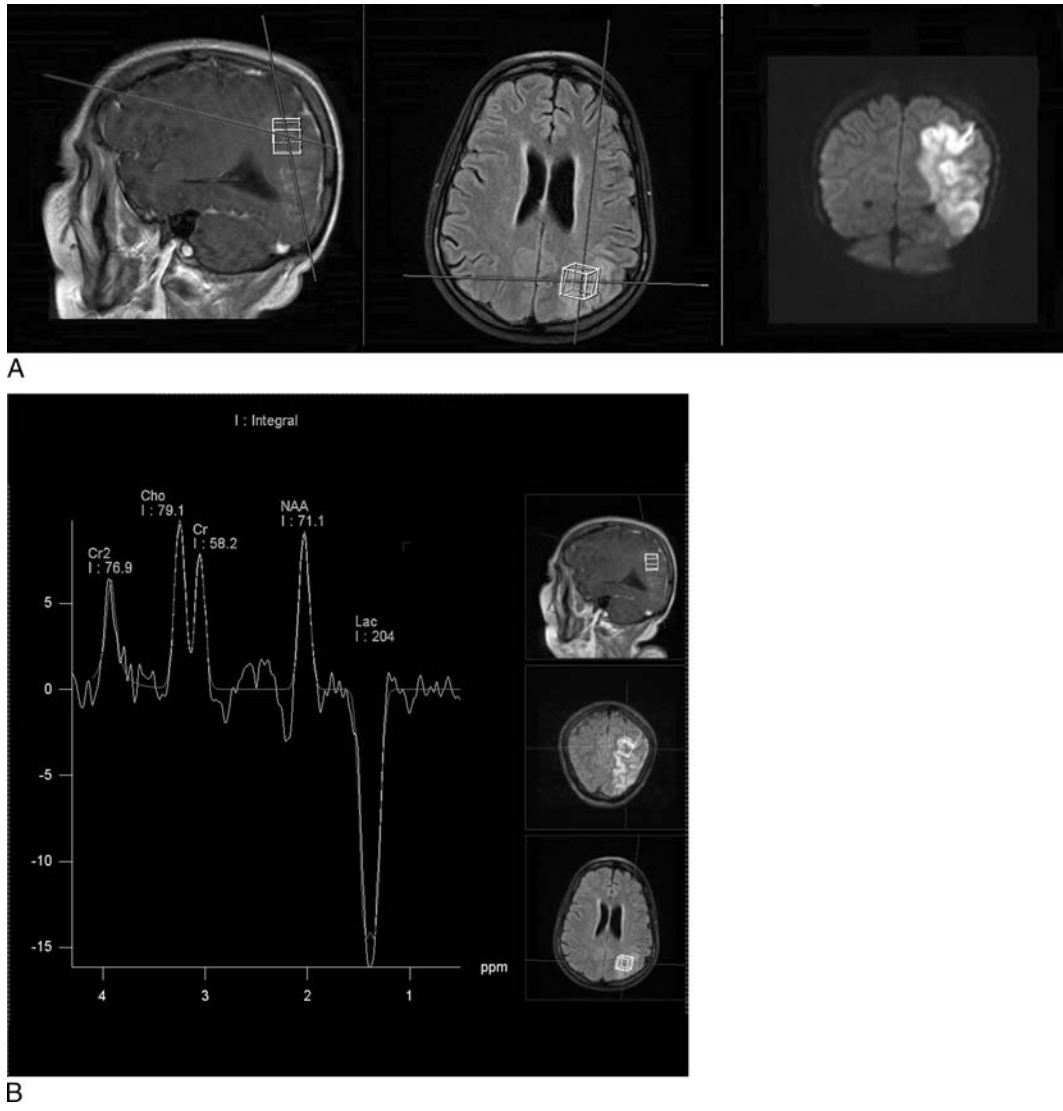

FIGURE 7. Magnetic resonance images (top row) and MRS (bottom row) of ischemia. Reduced NAA is depicted because of neuronal loss. The large lactate peak indicates anaerobic metabolism.

patients with lower $CD4^+$ lymph counts[130] and decreased after therapy.[131] N-acetyl-aspartate was found to be reduced already early during the course of the infection[132] and was even more pronounced with greater human immunodeficiency virus viremia.[130] In the first year of infection, increased Cho-Cr levels and reduced NAA levels were found that were correlated to increased $CD16^+$ count.[133] Despite therapy, there are reports of a persistent NAA reduction in chronically ill but stable patients,[134] whereas significantly decreased ratios were only found in patients with severe cognitive decline.[135]

Closing Remarks

Magnetic resonance spectroscopy is a powerful noninvasive tool that can assist clinical MRI. Although, in clinical routine, there are no absolute values and changes in certain metabolites that are not specific for certain disorders or tumor types for the most part, a change in their ratios compared with the healthy brain or during the course of the disease renders clinical imaging, and thus diagnosis, more valuable.

REFERENCES

1. Brandao LA, Domingues RC. *MR Spectroscopy of the Brain*. Philadelphia, PA: Lippincott Williams & Wilkins, 2004.
2. Bachert P, Schröder L. Magnetic resonance imaging spectroscopy. Part 1: basics [article in German]. *Radiologe*. 2003;43:1113–1126.
3. Bachert P, Lichy MP. Magnetic resonance spectroscopy. Part 2: application in diagnosis and clinical research [article in German]. *Radiologe*. 2004;44:81–95.
4. Backens M. Basic principles of MR spectroscopy [article in German]. *Radiologe*. 2010;50:767–774.
5. Kohler S. Single voxel proton brain exam. In: *Applications Guide Signa Advantage*. Schenectady, NY: General Electric Company, 1993.
6. Cousins JP. Clinical MR spectroscopy: fundamentals, current applications, and future potential. *AJR Am J Roentgenol*. 1995;164: 1337–1347.
7. Di Costanzo A, Trojsi F, Tosetti M, et al. Proton MR spectroscopy of the brain at 3 T: an update. *Eur Radiol*. 2007;17:1651–1662.
8. Lin A, Ross BD, Harris K, et al. Efficacy of proton magnetic resonance spectroscopy in neurological diagnosis and neurotherapeutic decision making. *NeuroRx*. 2005;2:197–214.
9. Sijens PE, Oudkerk M, Reijngoud DJ, et al. 1H MR chemical shift imaging detection of phenylalanine in patients suffering from phenylketonuria (PKU). *Eur Radiol*. 2004;14:1895–1900.
10. Sijens PE, Verbruggen KT, Meiners LC, et al. 1H chemical shift imaging of the brain in guanidino methyltransferase deficiency, a creatine deficiency syndrome; guanidinoacetate accumulation in the gray matter. *Eur Radiol*. 2005;15:1923–1926.
11. Huisman TA, Thiel T, Steinmann B, et al. Proton magnetic resonance spectroscopy of the brain of a neonate with nonketotic hyperglycinemia: in vivo-in vitro (ex vivo) correlation. *Eur Radiol*. 2002;12:858–861.
12. Kim JH, Chang KH, Na DG, et al. Comparison of 1.5T and 3T 1H MR spectroscopy for human brain tumors. *Korean J Radiol*. 2006;7: 156–161.
13. Danielsen ER, Ross B. *Magnetic Resonance Spectroscopy Diagnosis of Neurological Diseases*. New York, NY: Dekker, 1999.
14. Komoroski RA, Heimberg C, Cardwell D. Effects of gender and region on proton MRS of normal human brain. *Magn Reson Imaging*. 1999;17: 427–433.
15. Raininko R, Mattsson P. Metabolite concentrations in supraventricular white matter from teenage to early old age: a short echo time 1H magnetic resonance spectroscopy (MRS) study. *Acta Radiol*. 2010;51: 309–315.
16. Wilkinson ID, Paley MN, Miszkiel KA, et al. Cerebral volumes and spectroscopic proton metabolites on MR: is sex important? *Magn Reson Imaging*. 1997;15:243–248.
17. Jayasundar R, Raghunathan P. Evidence for left-right asymmetries in the proton MRS of brain in normal volunteers. *Magn Reson Imaging*. 1997; 15:223–234.
18. Marshall I, Wardlaw J, Cannon J, et al. Reproducibility of metabolite peak areas in 1H MRS of brain. *Magn Reson Imaging*. 1996;14:281–292.
19. Katz-Brull R, Lenkinski RE. Frame-by-frame PRESS 1H-MRS of the brain at 3 T: the effects of physiological motion. *Magn Reson Med*. 2004; 51:184–187.
20. Star-Lack JM, Adalsteinsson E, Gold GE, et al. Motion correction and lipid suppression for ^{1}H magnetic resonance spectroscopy. *Magn Reson Med*. 2000;43:325–330.
21. Zaitsev M, Speck O, Hennig J, et al. Single-voxel MRS with prospective motion correction and retrospective frequency correction. *NMR Biomed*. 2010;23:325–332.
22. Behar KL, den Hollander JA, Stromski ME, et al. High-resolution 1H nuclear magnetic resonance study of cerebral hypoxia in vivo. *Proc Natl Acad Sci U S A*. 1983;80:4945–4948.
23. Gadian DG, Proctor E, Williams SR, et al. Neurometabolic effects of an inborn error of amino acid metabolism demonstrated in vivo by 1H NMR. *Magn Reson Med*. 1986;3:150–156.
24. Urenjak J, Williams SR, Gadian DG, et al. Proton nuclear magnetic resonance spectroscopy unambiguously identifies different neural cell types. *J Neurosci*. 1993;13:981–989.
25. Blüml S, Wisnowski JL, Nelson MD Jr, et al. Metabolic maturation of the human brain from birth through adolescence: insights from in vivo magnetic resonance spectroscopy. *Cereb Cortex*. 2013;23:2944–2955.
26. Kreis R, Ernst T, Ross BD. Development of the human brain: *in vivo* quantification of metabolite and water content with proton magnetic resonance spectroscopy. *Magn Reson Med*. 1993;30:424–437.
27. Kimura H, Fujii Y, Itoh S, et al. Metabolic alterations in the neonate and infant brain during development: evaluation with proton MR spectroscopy. *Radiology*. 1995;194:483–489.
28. van der Knaap MS, van der Grond J, van Rijen PC, et al. Age-dependent changes in localized proton and phosphorus MR spectroscopy of the brain. *Radiology*. 1990;176:509–513.
29. Altman DI, Perlman JM, Volpe JJ. Cerebral oxygen metabolism in newborns. *Pediatrics*. 1993;92:99–104.
30. Leth H, Toft PB, Pryds O, et al. Brain lactate in preterm and growth-retarded neonates. *Acta Paediatr*. 1995;84:495–499.
31. Penrice J, Cady EB, Lorek A. Proton magnetic resonance spectroscopy of the brain in normal preterm and term infants, and early changes after perinatal hypoxia-ischemia. *Pediatr Res*. 1996;40:6–14.
32. Card D, Nossin-Manor R, Moore AM, et al. Brain metabolite concentrations are associated with illness severity scores and white matter abnormalities in very preterm infants. *Pediatr Res*. 2013;74:75–81.
33. Pouwels PJ, Brockmann K, Kruse B, et al. Regional age dependence of human brain metabolites from infancy to adulthood as detected by quantitative localized proton MRS. *Pediatr Res*. 1999;46:474–485.
34. Astley SJ, Richards T, Aylward EH, et al. Magnetic resonance spectroscopy outcomes from a comprehensive magnetic resonance study of children with fetal alcohol spectrum disorders. *Magn Reson Imaging*. 2009;27:760–778.
35. Cortese BM, Moore GJ, Bailey BA, et al. Magnetic resonance and spectroscopic imaging in prenatal alcohol-exposed children: preliminary findings in the caudate nucleus. *Neurotoxicol Teratol*. 2006;28:597–606.
36. Chang L, Cloak CC, Jiang CS, et al. Lower glial metabolite levels in brains of young children with prenatal nicotine exposure. *J Neuroimmune Pharmacol*. 2012;7:243–252.

37. Barkovich AJ, Westmark KD, Bedi HS, et al. Proton spectroscopy and diffusion imaging on the first day of life after perinatal asphyxia: preliminary report. *AJNR Am J Neuroradiol*. 2001;22:1786–1794.
38. Barkovich AJ, Miller SP, Bartha A, et al. MR imaging, MR spectroscopy, and diffusion tensor imaging of sequential studies in neonates with encephalopathy. *AJNR Am J Neuroradiol*. 2006;27:533–547.
39. Roelants-Van Rijn AM, van der Grond J, de Vries LS, et al. Value of (1)H-MRS using different echo times in neonates with cerebral hypoxia-ischemia. *Pediatr Res*. 2001;49:356–362.
40. Cheong JL, Cady EB, Penrice J, et al. Proton MR spectroscopy in neonates with perinatal cerebral hypoxic-ischemic injury: metabolite peak-area ratios, relaxation times, and absolute concentrations. *AJNR Am J Neuroradiol*. 2006;27:1546–1554.
41. Boichot C, Walker PM, Durand C, et al. Term neonate prognoses after perinatal asphyxia: contributions of MR imaging, MR spectroscopy, relaxation times, and apparent diffusion coefficients. *Radiology*. 2006; 239:839–848.
42. Hanrahan JD, Cox IJ, Azzopardi D, et al. Relation between proton magnetic resonance spectroscopy within 18 hours of birth asphyxia and neurodevelopment at 1 year of age. *Dev Med Child Neurol*. 1999;41: 76–82.
43. Hanrahan JD, Cox IJ, Edwards AD, et al. Persistent increases in cerebral lactate concentration after birth asphyxia. *Pediatr Res*. 1998;44:304–311.
44. Robertson NJ, Cox IJ, Cowan FM, et al. Cerebral intracellular lactic alkalosis persisting months after neonatal encephalopathy measured by magnetic resonance spectroscopy. *Pediatr Res*. 1999;46:287–296.
45. Martin E, Keller M, Ritter S, et al. Contribution of proton magnetic resonance spectroscopy to the evaluation of children with unexplained developmental delay. *Pediatr Res*. 2005;58:754–760.
46. Kosucu P, Erdemli S, Sönmez M, et al. MR spectroscopic evaluation of psychomotor delay of unknown cause in children. *AJR Am J Roentgenol*. 2010;194:1110–1115.
47. Filippi CG, Uluğ AM, Deck MD, et al. Developmental delay in children: assessment with proton MR spectroscopy. *AJNR Am J Neuroradiol*. 2002; 23:882–888.
48. Fayed N, Morales H, Modrego PJ, et al. White matter proton MR spectroscopy in children with isolated developmental delay: does it mean delayed myelination? *Acad Radiol*. 2006;13:229–235.
49. Corrigan NM, Shaw DW, Estes AM, et al. Atypical developmental patterns of brain chemistry in children with autism spectrum disorder. *JAMA Psychiatry*. 2013;70:964–974.
50. Limperopoulos C, Tworetzky W, McElhinney DB, et al. Brain volume and metabolism in fetuses with congenital heart disease: evaluation with quantitative magnetic resonance imaging and spectroscopy. *Circulation*. 2010;121:26–33.
51. Hardan AY, Minshew NJ, Melhem NM, et al. An MRI and proton spectroscopy study of the thalamus in children with autism. *Psychiatry Res*. 2008;163:97–105.
52. Mori K, Toda Y, Ito H, et al. A proton magnetic resonance spectroscopic study in autism spectrum disorders: amygdala and orbito-frontal cortex. *Brain Dev*. 2013;35:139–145.
53. Aoki Y, Kasai K, Yamasue H. Age-related change in brain metabolite abnormalities in autism: a meta-analysis of proton magnetic resonance spectroscopy studies. *Transl Psychiatry*. 2012;17:e69.
54. Vasconcelos MM, Brito AR, Domingues RC, et al. Proton magnetic resonance spectroscopy in school-aged autistic children. *J Neuroimaging*. 2008;18:288–295.
55. Corrigan NM, Shaw DW, Richards TL, et al. Proton magnetic resonance spectroscopy and MRI reveal no evidence for brain mitochondrial dysfunction in children with autism spectrum disorder. *J Autism Dev Disord*. 2012;42:105–115.
56. Ipser JC, Syal S, Bentley J, et al. 1H-MRS in autism spectrum disorders: a systematic meta-analysis. *Metab Brain Dis*. 2012;27:275–287.
57. Bianchi MC, Tosetti M, Battini R, et al. Proton MR spectroscopy of mitochondrial diseases: analysis of brain metabolic abnormalities and their possible diagnostic relevance. *AJNR Am J Neuroradiol*. 2003;24: 1958–1966.
58. De Stefano N, Matthews PM, Ford B, et al. Short-term dichloroacetate treatment improves indices of cerebral metabolism in patients with mitochondrial disorders. *Neurology*. 1995;45:1193–1198.
59. Jurkiewicz E, Chełstowska S, Pakuła-Kościesza I, et al. Proton MR spectroscopy in patients with leigh syndrome. *Neuroradiol J*. 2011;24: 424–428.
60. Krägeloh-Mann I, Grodd W, Schöning M, et al. Proton spectroscopy in five patients with Leigh's disease and mitochondrial enzyme deficiency. *Dev Med Child Neurol*. 1993;35:769–776.
61. Brockmann K, Dechent P, Meins M, et al. Cerebral proton magnetic resonance spectroscopy in infantile Alexander disease. *J Neurol*. 2003; 250:300–306.
62. van der Voorn JP, Pouwels PJ, Salomons GS, et al. Unraveling pathology in juvenile Alexander disease: serial quantitative MR imaging and spectroscopy of white matter. *Neuroradiology*. 2009;51:669–675.
63. Grodd W, Krägeloh-Mann I, Petersen D, et al. In vivo assessment of N-acetylaspartate in brain in spongy degeneration (Canavan's disease) by proton spectroscopy. *Lancet*. 1990;336:437–438.
64. Barker PB, Bryan RN, Kumar AJ, et al. Proton NMR spectroscopy of Canavan's disease. *Neuropediatrics*. 1992;23:263–267.
65. Mochel F, Boildieu N, Barritault J, et al. Elevated CSF N-acetylaspartylglutamate suggests specific molecular diagnostic abnormalities in patients with white matter diseases. *Biochim Biophys Acta*. 2010;1802:1112–1117.
66. Hanefeld FA, Brockmann K, Pouwels PJ, et al. Quantitative proton MRS of Pelizaeus-Merzbacher disease: evidence of dys- and hypomyelination. *Neurology*. 2005;65:701–706.
67. Razek AA, Abdalla A, Gaber NA, et al. Proton MR Spectroscopy of the brain in children with neuronopathic Gaucher's disease. *Eur Radiol*. 2013;23:3005–3011.
68. Carpentier A, Galanaud D, Puybasset L, et al. Early morphologic and spectroscopic magnetic resonance in severe traumatic brain injuries can detect "invisible brain stem damage" and predict "vegetative states". *J Neurotrauma*. 2006;23:674–685.
69. Cohen BA, Inglese M, Rusinek H, et al. Proton MR spectroscopy and MRI-volumetry in mild traumatic brain injury. *AJNR Am J Neuroradiol*. 2007;28:907–913.
70. Yeo RA, Phillips JP, Jung RE, et al. Magnetic resonance spectroscopy detects brain injury and predicts cognitive functioning in children with brain injuries. *J Neurotrauma*. 2006;23:1427–1435.
71. Aaen GS, Holshouser BA, Sheridan C, et al. Magnetic resonance spectroscopy predicts outcomes for children with nonaccidental trauma. *Pediatrics*. 2010;125:295–303.
72. Remy C, Von Kienlin M, Lotito S, et al. In vivo 1H NMR spectroscopy of an intracerebral glioma in the rat. *Magn Reson Med*. 1989;9: 395–401.
73. Bárány M, Langer BG, Glick RP, et al. In vivo H-1 spectroscopy in humans at 1.5 T. *Radiology*. 1988;167:839–844.
74. Luyten PR, Marien AJ, Heindel W, et al. Metabolic imaging of patients with intracranial tumors: H-1 MR spectroscopic imaging and PET. *Radiology*. 1990;176:791–799.
75. Bruhn H, Frahm J, Gyngell ML, et al. Noninvasive differentiation of tumors with use of localized H-1 MR spectroscopy in vivo: initial experience in patients with cerebral tumors. *Radiology*. 1989;172: 541–548.

76. Sostman HD, Charles HC. Noninvasive differentiation of tumors with use of localized H-1 spectroscopy in vivo: initial experience in patients with cerebral tumors. *Invest Radiol*. 1990;25:1047–1050.
77. Arnold DL, Shoubridge EA, Villemure JG, et al. Proton and phosphorus magnetic resonance spectroscopy of human astrocytomas in vivo. Preliminary observations on tumor grading. *NMR Biomed*. 1990;3: 184–189.
78. Gill SS, Thomas DG, Van Bruggen N, et al. Proton MR spectroscopy of intracranial tumours: in vivo and in vitro studies. *J Comput Assist Tomogr*. 1990;14:497–504.
79. Ishimaru H, Morikawa M, Iwanaga S, et al. Differentiation between high-grade glioma and metastatic brain tumor using single-voxel proton MR spectroscopy. *Eur Radiol*. 2001;11:1784–1791.
80. Sijens PE, Levendag PC, Vecht CJ, et al. 1H MR spectroscopy detection of lipids and lactate in metastatic brain tumors. *NMR Biomed*. 1996;9: 65–71.
81. Shimizu H, Kumabe T, Tominaga T, et al. Noninvasive evaluation of malignancy of brain tumors with proton MR spectroscopy. *AJNR Am J Neuroradiol*. 1996;17:737–747.
82. Tong Z, Yamaki T, Harada K, et al. In vivo quantification of the metabolites in normal brain and brain tumors by proton MR spectroscopy using water as an internal standard. *Magn Reson Imaging*. 2004;22: 1017–1024.
83. Hattingen E, Raab P, Franz K, et al. Prognostic value of choline and creatine in WHO grade II gliomas. *Neuroradiology*. 2008;50:759–767.
84. Wattjes MP, Harzheim M, Lutterbey GG, et al. Axonal damage but no increased glial cell activity in the normal-appearing white matter of patients with clinically isolated syndromes suggestive of multiple sclerosis using high-field magnetic resonance spectroscopy. *AJNR Am J Neuroradiol*. 2007;28:1517–1522.
85. Hollingworth W, Medina LS, Lenkinski RE, et al. A systematic literature review of magnetic resonance spectroscopy for the characterization of brain tumors. *AJNR Am J Neuroradiol*. 2006;27:1404–1411.
86. McKnight TR, von dem Bussche MH, Vigneron DB, et al. Histopathological validation of a three-dimensional magnetic resonance spectroscopy index as a predictor of tumor presence. *J Neurosurg*. 2002; 97:794–802.
87. Law M, Yang S, Wang H, et al. Glioma grading: sensitivity, specificity, and predictive values of perfusion MR imaging and proton MR spectroscopic imaging compared with conventional MR imaging. *AJNR Am J Neuroradiol*. 2003;24:1989–1998.
88. Crawford FW, Khayal IS, McGue C, et al. Relationship of pre-surgery metabolic and physiological MR imaging parameters to survival for patients with untreated GBM. *J Neurooncol*. 2009;91:337–351.
89. Porto L, Kieslich M, Franz K, et al. Proton magnetic resonance spectroscopic imaging in pediatric low-grade gliomas. *Brain Tumor Pathol*. 2010;27:65–70.
90. Senft C, Hattingen E, Pilatus U, et al. Diagnostic value of proton magnetic resonance spectroscopy in the noninvasive grading of solid gliomas: comparison of maximum and mean choline values. *Neurosurgery*. 2009; 65:908–913.
91. Hattingen E, Delic O, Franz K, et al. (1)H MRSI and progression-free survival in patients with WHO grades II and III gliomas. *Neurol Res*. 2010;32:593–602.
92. Server A, Kulle B, Gadmar ØB, et al. Measurements of diagnostic examination performance using quantitative apparent diffusion coefficient and proton MR spectroscopic imaging in the preoperative evaluation of tumor grade in cerebral gliomas. *Eur J Radiol*. 2011;80: 462–470.
93. Segebarth CM, Balériaux DF, Luyten PR, et al. Detection of metabolic heterogeneity of human intracranial tumors in vivo by 1H NMR spectroscopic imaging. *Magn Reson Med*. 1990;13:62–76.
94. Chawla S, Zhang Y, Wang S, et al. Proton magnetic resonance spectroscopy in differentiating glioblastomas from primary cerebral lymphomas and brain metastases. *J Comput Assist Tomogr*. 2010;34: 836–841.
95. Yamasaki F, Kurisu K, Kajiwara Y, et al. Magnetic resonance spectroscopic detection of lactate is predictive of a poor prognosis in patients with diffuse intrinsic pontine glioma. *Neuro Oncol*. 2011;13: 791–801.
96. Steffen-Smith EA, Shih JH, Hipp SJ, et al. Proton magnetic resonance spectroscopy predicts survival in children with diffuse intrinsic pontine glioma. *J Neurooncol*. 2011;105:365–373.
97. Stadlbauer A, Buchfelder M, Doelken MT, et al. Magnetic resonance spectroscopic imaging for visualization of the infiltration zone of glioma. *Cent Eur Neurosurg*. 2011;72:63–69.
98. Guillevin R, Menuel C, Taillibert S, et al. Predicting the outcome of grade II glioma treated with temozolomide using proton magnetic resonance spectroscopy. *Br J Cancer*. 2011;104:1854–1861.
99. Constans JM, Collet S, Kauffmann F, et al. Five-year longitudinal MRI follow-up and (1)H single voxel MRS in 14 patients with gliomatosis treated with temodal, radiotherapy and antiangiogenic therapy. *Neuroradiol J*. 2011;24:401–414.
100. Quon H, Brunet B, Alexander A, et al. Changes in serial magnetic resonance spectroscopy predict outcome in high-grade glioma during and after postoperative radiotherapy. *Anticancer Res*. 2011;31:3559–3565.
101. Kim H, Catana C, Ratai EM, et al. Serial magnetic resonance spectroscopy reveals a direct metabolic effect of cediranib in glioblastoma. *Cancer Res*. 2011;71:3745–3752.
102. Fink JR, Carr RB, Matsusue E, et al. Comparison of 3 Tesla proton MR spectroscopy, MR perfusion and MR diffusion for distinguishing glioma recurrence from posttreatment effects. *J Magn Reson Imaging*. 2012;35:56–63.
103. Smith EA, Carlos RC, Junck LR, et al. Developing a clinical decision model: MR spectroscopy to differentiate between recurrent tumor and radiation change in patients with new contrast-enhancing lesions. *AJR Am J Roentgenol*. 2009;192:W45–W52.
104. Weybright P, Sundgren PC, Maly P, et al. Differentiation between brain tumor recurrence and radiation injury using MR spectroscopy. *AJR Am J Roentgenol*. 2005;185:1471–1476.
105. Ulmer S, Helle M, Jansen O, et al. Intraoperative dynamic susceptibility contrast weighted magnetic resonance imaging (iDSC-MRI) - Technical considerations and feasibility. *Neuroimage*. 2009;45:38–43.
106. Ulmer S, Hartwigsen G, Riedel C, et al. Intraoperative dynamic susceptibility contrast MRI (iDSC-MRI) is as reliable as preoperatively acquired perfusion mapping. *Neuroimage*. 2010;49:2158–2162.
107. Pamir MN, Özduman K, Yıldız E, et al. Intraoperative magnetic resonance spectroscopy for identification of residual tumor during low-grade glioma surgery: clinical article. *J Neurosurg*. 2013;118: 1191–1198.
108. O'Neill J, Schuff N, Marks WJ Jr, et al. Quantitative 1H magnetic resonance spectroscopy and MRI of Parkinson's disease. *Mov Disord*. 2002;17:917–927.
109. Metarugcheep P, Hanchaiphiboolkul S, Viriyavejakul A, et al. The usage of proton magnetic resonance spectroscopy in Parkinson's disease. *J Med Assoc Thai*. 2012;95:949–952.
110. Gröger A, Chadzynski G, Godau J, et al. Three-dimensional magnetic resonance spectroscopic imaging in the substantia nigra of healthy controls and patients with Parkinson's disease. *Eur Radiol*. 2011;21: 1962–1969.
111. Guevara CA, Blain CR, Stahl D, et al. Quantitative magnetic resonance spectroscopic imaging in Parkinson's disease, progressive supranuclear palsy and multiple system atrophy. *Eur J Neurol*. 2010;17: 1193–1202.

112. Modrego PJ, Fayed N, Artal J, et al. Correlation of findings in advanced MRI techniques with global severity scales in patients with Parkinson disease. *Acad Radiol*. 2011;18:235–241.
113. Hattingen E, Magerkurth J, Pilatus U, et al. Phosphorus and proton magnetic resonance spectroscopy demonstrates mitochondrial dysfunction in early and advanced Parkinson's disease. *Brain*. 2009; 132(pt 12):3285–3297.
114. Griffith HR, den Hollander JA, Okonkwo OC, et al. Brain metabolism differs in Alzheimer's disease and Parkinson's disease dementia. *Alzheimers Dement*. 2008;4:421–427.
115. Griffith HR, den Hollander JA, Okonkwo OC, et al. Brain N-acetylaspartate is reduced in Parkinson disease with dementia. *Alzheimer Dis Assoc Disord*. 2008;22:54–60.
116. Griffith HR, Okonkwo OC, O'Brien T, et al. Reduced brain glutamate in patients with Parkinson's disease. *NMR Biomed*. 2008;21: 381–387.
117. Camicioli RM, Hanstock CC, Bouchard TP, et al. Magnetic resonance spectroscopic evidence for presupplementary motor area neuronal dysfunction in Parkinson's disease. *Mov Disord*. 2007;22: 382–386.
118. Nie K, Zhang Y, Huang B, et al. Marked N-acetylaspartate and choline metabolite changes in Parkinson's disease patients with mild cognitive impairment. *Parkinsonism Relat Disord*. 2013;19:329–334.
119. Pagonabarraga J, Gómez-Ansón B, Rotger R, et al. Spectroscopic changes associated with mild cognitive impairment and dementia in Parkinson's disease. *Dement Geriatr Cogn Disord*. 2012;34:312–318.
120. Summerfield C, Gómez-Ansón B, Tolosa E, et al. Dementia in Parkinson disease: a proton magnetic resonance spectroscopy study. *Arch Neurol*. 2002;59:1415–1420.
121. Oz G, Alger JR, Barker PB, et al. Clinical proton MR spectroscopy in central nervous system disorders. *Radiology*. 2014;270:658–679.
122. van der Toorn A, Verheul HB, Berkelbach van der Sprenkel JW, et al. Changes in metabolites and tissue water status after focal ischemia in cat brain assessed with localized proton MR spectroscopy. *Magn Reson Med*. 1994;32:685–691.
123. Sager TN, Laursen H, Hansen AJ. Changes in N-acetyl-aspartate content during focal and global brain ischemia of the rat. *J Cereb Blood Flow Metab*. 1995;15:639–646.
124. Qian J, Qian B, Lei H. Reversible loss of N-acetylaspartate after 15-min transient middle cerebral artery occlusion in rat: a longitudinal study with in vivo proton magnetic resonance spectroscopy. *Neurochem Res*. 2013;38:208–217.
125. Berthet C, Lei H, Gruetter R, et al. Early predictive biomarkers for lesion after transient cerebral ischemia. *Stroke*. 2011;42:799–805.
126. Cirstea CM, Brooks WM, Craciunas SC, et al. Primary motor cortex in stroke: a functional MRI-guided proton MR spectroscopic study. *Stroke*. 2011;42:1004–1009.
127. Craciunas SC, Brooks WM, Nudo RJ, et al. Motor and premotor cortices in subcortical stroke: proton magnetic resonance spectroscopy measures and arm motor impairment. *Neurorehabil Neural Repair*. 2013;27: 411–420.
128. Zhang M, Lu J, Jiao L, et al. Proton magnetic resonance spectroscopy in patients with symptomatic unilateral internal carotid artery / middle cerebral artery stenosis or occlusion. *J Magn Reson Imaging*. 2011;34: 910–916.
129. Valcour V, Chalermchai T, Sailasuta N, et al. Central nervous system viral invasion and inflammation during acute HIV infection. *J Infect Dis*. 2012;206:275–282.
130. Winston A, Duncombe C, Li PC, et al. Two patterns of cerebral metabolite abnormalities are detected on proton magnetic resonance spectroscopy in HIV-infected subjects commencing antiretroviral therapy. *Neuroradiology*. 2012;54:1331–1339.
131. Sailasuta N, Ross W, Ananworanich J, et al. Change in brain magnetic resonance spectroscopy after treatment during acute HIV infection. *PLoS One*. 2012;7:e49272.
132. Lentz MR, Kim WK, Lee V, et al. Changes in MRS neuronal markers and T cell phenotypes observed during early HIV infection. *Neurology*. 2009;72:1465–1472.
133. Lentz MR, Kim WK, Kim H, et al. Alterations in brain metabolism during the first year of HIV infection. *J Neurovirol*. 2011;17:220–229.
134. Cysique LA, Moffat K, Moore DM, et al. HIV, vascular and aging injuries in the brain of clinically stable HIV-infected adults: a (1)H MRS study. *PLoS One*. 2013;8:e61738.
135. Harezlak J, Buchthal S, Taylor M, et al. Persistence of HIV-associated cognitive impairment, inflammation, and neuronal injury in era of highly active antiretroviral treatment. *AIDS*. 2011;25:625–633.